Chemical Physics Impact 11 (2025) 100910

Contents lists available at ScienceDirect

Chemical Physics Impact

journal homepage: www.sciencedirect.com/journal/chemical-physics-impact

Full Length Article

Enhanced solar energy harvest in dye-sensitized solar cells using silver-doped TiO_2 Photoelectrodes *via* Spray Pyrolysis

Piranave Sritharan [a,b], Meena Senthilnanthanan [a,*], Punniamoorthy Ravirajan [b], Dhayalan Velauthapillai [c,*], Gamaralalage Rajanya Asoka Kumara [d], Balraju Palanisamy [e]

[a] Department of Chemistry, University of Jaffna, Jaffna, 40000, Sri Lanka
[b] Clean Energy Research Laboratory, Department of Physics, University of Jaffna, Jaffna, 40000, Sri Lanka
[c] Faculty of Engineering and Science, Western Norway University of Applied Sciences, P.O. Box 7030, 5020, Bergen, Norway
[d] National Institute of Fundamental Studies, Hantana Road, Kandy, 20000, Sri Lanka
[e] Department of Physics, Coimbatore Institute of Technology, Coimbatore, 641 014, Tamil Nadu, India

ARTICLE INFO

Keywords:
Dssc
Spray pyrolysis
Ag-doped tio2
Hydrothermal synthesis
TTIP
PCE

ABSTRACT

This study focuses on doping TiO_2 with trace amounts of Ag^+ ions, employing spray pyrolysis to prepare the Ag-doped TiO_2 photoelectrode for application in Dye-Sensitized Solar Cells (DSSCs). In this regard, Ag-doped TiO_2 nanomaterials were initially synthesized from Titanium(IV) isopropoxide (TTIP) with varying concentrations of Silver nitrate ($AgNO_3$). The structural and optical characterizations of the synthesized nanomaterials confirmed the presence of TiO_2 in pure anatase phase and enhanced light absorption, respectively. The morphological characterization of Ag-doped TiO_2 nanomaterials revealed spherical shaped particles. Subsequently, the DSSCs were fabricated using Ruthenium-based N719 dye and imidazolium iodide/ triiodide redox couple as the sensitizer and electrolyte, respectively. Photovoltaic performances were evaluated under simulated solar irradiation (100 mW cm^{-2}, 1 sun, AM 1.5). The optimized device with 3 mmol % Ag-doped TiO_2 photoelectrode exhibited PCE (η) of 8.32 %, which was about 13 % greater than the device with un-doped TiO_2 (η = 7.35 %). The observed upsurge in PCE is due to the 10 % increase in short-circuit current density (J_{SC}) value resulting from enhancement in visible light absorption which was confirmed by UV–Visible spectroscopic analysis. Moreover, an improved electron transport in the Ag-doped TiO_2 based device was confirmed by electrochemical impedance spectroscopic study which is ascribed to the significant reduction in charge recombination. These findings demonstrate the potential of Ag-doped TiO_2 for enhanced DSSC performance, offering a viable pathway for improving solar energy conversion efficiency.

1. Introduction

The Dye-Sensitized Solar Cells (DSSCs) are becoming increasingly important, compared to traditional silicon-based solar cells, for eco-friendly, sustainable and energy-efficient industrial applications. The salient features of DSSCs, such as low-cost production, design flexibility, semi-transparent nature and excellent performance under indoor or diffuse lighting conditions, immensely contribute to integrating the same into smart windows, building facades and powering low-energy portable electronic devices. DSSCs consist of a mesoporous semiconductor photoelectrode sensitized by a dye, a redox electrolyte, and a counter electrode. The dye molecules in the photoelectrode harvest sunlight and generate excited electrons, which are then transferred through the semiconductor and external circuit to the counter electrode, producing electricity while the redox electrolyte reduces the oxidized dye molecules. Even though photoelectrode plays a major role in light harvesting and charge transport processes in these devices, poor visible light harvest, slow charge transport and recombination of the injected electrons limit the performance of the DSSCs. Various inorganic semiconductors, such as TiO_2 [1], ZnO [2], SnO_2 [3], and Nb_2O_5 [4], have been investigated as the photoelectrode material for DSSCs. Among them, TiO_2 is found to be a promising nanomaterial for sustainable energy generation primarily because of its cost-effectiveness, non-toxic properties, and remarkable stability. However, the efficiency of DSSCs is impeded by the narrow range of solar light absorption around 380 nm due to wide direct bandgap of TiO_2 (3.2 eV) and slow electron transport

* Corresponding authors.
E-mail addresses: meena@univ.jfn.ac.lk (M. Senthilnanthanan), Dhayalan.Velauthapillai@hvl.no (D. Velauthapillai).

https://doi.org/10.1016/j.chphi.2025.100910
Received 25 March 2025; Received in revised form 20 May 2025; Accepted 26 June 2025
Available online 3 July 2025

that leads to relaxation or recombination of charge carriers. In contrast most light-absorbing materials possess an absorption range between 500 and 600 nm which resulting in the wastage of significant portion of light. Nevertheless, the inherently wide bandgap of TiO_2 presents an opportunity to tailor its bandgap to a more favorable range through modification [5]. It has been reported that incorporating transition metals into TiO_2 nanomaterial leads to the creation of new energy levels possessing partially filled d-orbitals closer to the conduction band (CB) of TiO_2. These new energy levels improve absorption of solar light in the visible region by inducing a reduction in the bandgap. Also, the replacement of Ti^{4+} ion with transition metal cations while doping impacts dye adsorption due to varying binding affinities between the dye molecules and the doped transition metals [6]. Several transition metals, such as Chromium (Cr) [7], Manganese (Mn) [8], Iron (Fe) [9], Cobalt (Co) [10], Nickel (Ni) [11], Copper (Cu) [12], Zinc (Zn) [13], Ruthenium (Ru) [14], Tungsten (W) [15], Silver (Ag) [16], *etc.*, have been studied as dopants for TiO_2 nanomaterials with the aim of enhancing the power conversion efficiency of DSSCs.

The focus of this paper is on Ag-doped TiO_2 as it possesses reduced bandgap, retarded charge recombination and greater surface area for dye adsorption. Luo (2014) has reported 5.85 % efficiency for DSSC by employing screen printed tri-layered titania film implanted with 1×10^{16} atoms/cm^2 Ag^+ ions [17]. In another study, 1 % Ag-doped TiO_2 films, prepared by dip coating method, were found to increase the power conversion efficiency of DSSCs by 4.4 % over the un-doped TiO_2 films [18]. In a separate study, the Ag-doped TiO_2 photoelectrode was prepared by doctor blading method. The corresponding DSSC demonstrated an enhanced J_{SC} value compared to the control device due to a red shift towards increased visible light absorption and enhanced electron life time [19].

According to the previous studies, Ag-doping is found to improve dye adsorption, reduce charge-transfer resistance, and shift the conduction band edge resulting in enhanced photovoltaic performance. Building on these findings, this study explores the effect of Ag-doped TiO_2 photoelectrodes fabricated via spray pyrolysis with a focus on improving the power conversion efficiency and charge transport properties of DSSCs. The spray pyrolysis method was chosen to coat the nanomaterials on the substrate as the said method possesses better control over the thickness of TiO_2 film and uniform distribution of nanoparticles could be achieved by adjusting the parameters, such as nozzle size of spray gun, distance between the spray gun and FTO glass substrate, pressure exerted by air compressor, and concentration of Ag-doped TiO_2 colloidal solution. Furthermore, only minimal quantities of $AgNO_3$ were used as a dopant in this study, compared to the larger amounts reported in previous research [18–21].

The use of the spray pyrolysis method for coating Ag-doped TiO_2 nanomaterials is relatively uncommon in the existing literature. Moreover, this approach employs only a trace amount of silver as a dopant, which minimizes potential material cost and toxicity concerns while still achieving significant enhancement in photovoltaic performance. This combination of spray coating technique and minimal dopant usage highlights the novelty of this study.

2. Materials and methods

2.1. Materials

All materials, reagents, and solvents used in this research study were purchased from commercial sources; Fluorene-doped Tin Oxide coated glass (FTO glass) (13 Ω/cm^2, Sigma-Aldrich, USA), Titanium(IV) isopropoxide (TTIP) (≥98 %, Sigma-Aldrich, USA), Silver nitrate (ACS grade, VWR Chemicals, France), Absolute ethanol (VWR Chemicals, France), Acetic acid (≥99.8 %, Sigma-Aldrich, USA), Triton X-100 (laboratory grade, Acros Organics, USA), Di-tetrabutylammonium*cis*-bis (isothiocyanato)bis(2,2′-bipyridyl-4,4′-dicarboxylato)ruthenium(II) dye (N719 dye) (95 %, Sigma-Aldrich, USA), Acetonitrile (≥99.9 %, Sigma-Aldrich, USA), *tert*-Butyl alcohol (≥99.7 %, Sigma-Aldrich, USA), Dimethyl sulphoxide (≥99.9 %, Sigma-Aldrich, USA)

2.2. Methods

2.2.1. Synthesis of un-doped & ag-doped tio$_2$ colloidal solutions

Un-doped TiO_2 colloidal solution was synthesized by adopting the method employed by Mudiyanselage Sakunthala Pubudu Kumari Kumarasinghe [22]. 8.0 mL of TTIP and 1.0 mL of acetic acid were mixed with 8.0 mL of ethanol and steam was passed through the resulting solution to aid rapid hydrolysis. The expulsion of ethanol by steaming produced a transparent solid mass consisting of TiO_2 nanoparticles. The resultant solid mass was ground with 20.0 mL of de-ionized water in a motor and sonicated for 10 min. Finally, the dispersion was autoclaved at 150 °C for 3 hrs.

For the synthesis of varied concentrations of Ag-doped TiO_2 colloidal solutions, 8.0 mL of TTIP and 1.0 mL of acetic acid were mixed with 8.0 mL ethanol, followed by addition of varied amounts of $AgNO_3$ in dimethyl sulphoxide and the resulting individual solutions were stirred well before passing steam. The resultant TiO_2 nanoparticles doped with varied amounts of Ag were ground separately with 20.0 mL of de-ionized water in a motor and sonicated for 10 min. Finally, the individual dispersions were autoclaved at 150 °C for 3 hrs.

2.2.2. Fabrication of un-doped & ag-doped tio$_2$ photoelectrodes

Fabrication of un-doped & Ag-doped TiO_2 photoelectrodes was also carried out by adopting the method employed by Mudiyanselage Sakunthala Pubudu Kumari Kumarasinghe [22]. FTO glass was cut into 1 cm x 2 cm pieces and ultrasonically cleaned with soap water, deionized water and ethanol. The synthesized 30.0 mL of un-doped or each of Ag-doped colloidal TiO_2 precursor solutions, 8.25 mL of acetic acid, 8 drops of Triton X-100 and 30.0 mL of ethanol were mixed thoroughly to prepare the un-doped or the corresponding Ag-doped TiO_2 precursors. The precursor suspensions were sprayed separately on pre-heated (150 °C) FTO glass substrates using a hand-made spray gun. Then, the FTO glass substrates coated with the un-doped or varied amounts of Ag-doped TiO_2 precursors were sintered at 500 °C for 30 min in air to crystallize TiO_2 and remove organic residues, allowed to cool down to 80 °C and soaked into 0.3 mmoldm^{-3} solution of N719 dye dissolved in a 1:1 (v/v) mixture of acetonitrile and *tert*-butyl alcohol. The sensitization process was carried out at room temperature under dark for 15 hrs. to ensure maximum dye adsorption for better light absorption.

2.2.3. Assembling dye-sensitized solar cells

The resultant dye-sensitized un-doped and Ag-doped TiO_2 photoelectrodes were rinsed in acetonitrile to remove excess unanchored dye molecules. The Platinum (Pt) coated FTO glass was used as counter electrode and individually assembled with the dye adsorbed photoelectrodes. Subsequently, a small amount of imidazolium iodide/ triiodide electrolyte was injected between the two electrodes of the individual cell. Finally, the cell was masked by maintaining the active area of the photoelectrode as 0.25 cm^2.

3. Characterization

The structural, optical and morphological characterizations were performed on the synthesized un-doped and Ag-doped TiO_2 electrode. The X-ray Diffraction analysis utilized the Cu-K_α radiation (wavelength 0.15406 nm) (PANalytical-AERIS, Almelo, Netherlands) and encompassed a scan range (2θ) spanning from 10 to 90 degrees, with a step size of 0.0027 degrees and a scan speed of 4 °/min. The Energy-Dispersive X-ray spectroscopy (Bruker EDS Analyzer) was employed to identify the elemental composition of the synthesized nanomaterials. Brunauer-Emmett-Teller (BET) analysis was carried out to study the surface area and pore volume of TiO_2 nanomaterials (Micromeritics, ASAP 2460, USA).

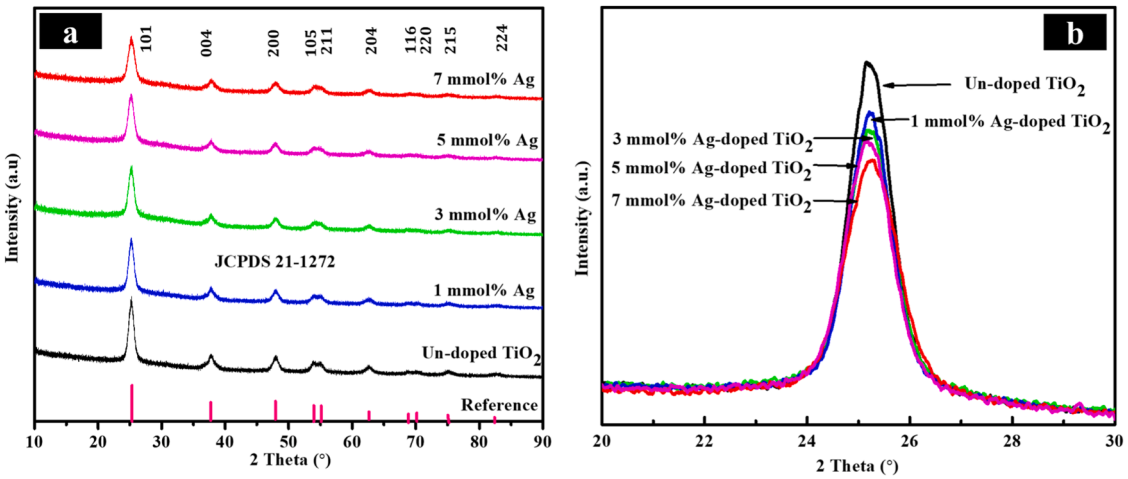

Fig. 1. (a) XRD patterns and (b) Expanded high intensity peak of Un-doped, 1, 3, 5, 7 mmol % Ag-doped TiO_2 nanomaterials.

The optical properties of the synthesized un-doped & Ag-doped TiO_2 photoelectrode (before and after dye adsorption) were examined using Double Beam UV–Visible spectrophotometer (JENWAY 6800, OSA, UK). The surface morphology of the fabricated films was studied using Field-Emission Scanning Electron Microscopy (Carl ZEISS (SIGMA), UK).

Initially, the PV performances of the DSSCs fabricated with varying concentrations (1, 3, 5, and 7 mmol %) of Ag-doped TiO_2 based photoelectrodes were studied and the optimum PCE was observed for the device comprised of 3 mmol % Ag-doped TiO_2. Hence, the IPCE analysis was carried out for the un-doped and 3 mmol % Ag-doped TiO_2 only whereas EIS and EDX analyses were conducted on the un-doped, as well as 3 and 7 mmol % Ag-doped TiO_2-based DSSCs.

4. Results and discussion

4.1. Structural characterization

4.1.1. X-Ray diffraction (XRD) spectroscopy

The XRD analysis was conducted on the synthesized TiO_2 nanomaterials, both un-doped and doped with 1, 3, 5 and 7 mmol % of Ag. Fig. 1(a) illustrates the diffraction patterns and crystal structures. The recorded peaks at 2θ values of 25.2°, 37.6°, 48.2°, 53.7°, 55.0°, 62.5°, 68.5°, 70.2°, 74.8°, and 82 0.5° correspond to the reflection planes of (101), (004), (200), (105), (211), (204), (116), (220), (215), and (224), respectively. The presence of a clearly defined pure anatase TiO_2 phase has been verified, as indicated by the Anatase XRD JCPDS Card No 21–1272.

The XRD analysis of the synthesized Ag-doped TiO_2 nanomaterials reveals peaks corresponding to the anatase phase of TiO_2 even after incorporation of silver. However, the reflection pattern of silver was not detected due to its presence in extremely low quantities in the synthesized nanomaterials [17].

The Debye-Scherrer equation, given below, was employed to determine the average crystallite size of crystalline anatase TiO_2:

$$d = \frac{k\lambda}{\beta cos\theta}$$

where k is a dimensionless shape factor (typically around 0.89), λ is the wavelength of the X-ray beam (0.15406 nm), θ is the Bragg angle, and β is the full width at half maximum (FWHM) calculated from the predominant anatase (101) plane. Using the above equation, the estimated crystallite sizes of the un-doped, 1, 3, 5 and 7 mmol % Ag-doped TiO_2 were determined. According to the Scherrer equation, crystallite size (d) is inversely related to peak broadening (β). In other words, smaller crystallites lead to broader diffraction peaks, while larger crystallites result in narrower peaks (Fig. 1(b)) [23,24]. These findings indicate that Ag doping leads to a decrease in the crystallite size of TiO_2 nanomaterials. A similar finding has been reported by Gupta [19]. The decrease in crystallite size of TiO_2 due to Ag doping may enhance dye adsorption as a result of increased surface area of the synthesized Ag-doped TiO_2 nanomaterials.

Table 1
Physicochemical characteristics of Un-doped, and Ag-doped TiO_2 nanomaterials.

Ag (mmol %)	Crystallite Size (nm)	Micro strain x 10^{-3}	Dislocation Density (nm^{-2} x 10^{-3})	Crystallinity (%)
0	7.64	20.05	17.09	62.82
1	7.54	20.28	17.54	62.07
3	7.10	21.59	19.84	59.23
5	6.92	22.14	20.89	58.68
7	6.20	24.77	25.93	55.03

The Micro strain of the nanomaterials was calculated using Williamson–Hall (W–H) method.

$$\beta cos\theta = \varepsilon 4 sin\theta + \frac{0.89\lambda}{d}$$

Where λ is the wavelength of X-ray radiation, β is FWHM, and θ is the Bragg angle of the diffraction peaks, d is crystallite size with micro strain and ε is the effective value of the micro strain. When βcos θ plotted against 4 sin θ, the slope gives the value of micro strain. The dislocation density of both undoped and Ag-doped TiO_2 nanomaterials was calculated using the relation ($1/d^2$), where d represents the average crystallite size. This parameter plays a crucial role in determining the electrical and mechanical properties of nanomaterials. A higher dislocation density typically indicates a harder material [5]. Furthermore, the crystallinity of Ag-doped TiO_2 tends to decrease with increasing silver content. This reduction is attributed to the differences in ionic size and electronic structure between Ag^+ and Ti^{4+}, which introduce defects and disrupt the regular crystal lattice. Consequently, these structural disturbances induce micro strain within the TiO_2 crystal structure. Calculated crystallite size, micro strain, dislocation density and crystallinity of un-doped and Ag-doped TiO_2 nanomaterials are listed in Table 1.

4.1.2. Energy-Dispersive X-ray (EDX) spectroscopy

Fig. 2 depicts the elemental compositions of un-doped, 3 mmol % Ag-doped and 7 mmol % Ag-doped TiO_2 electrodes. The atomic percentages of elements present in TiO_2 electrodes are presented in Table 2. The presence of Ag in EDX mapping in Fig. 2(b & c) confirms the successful

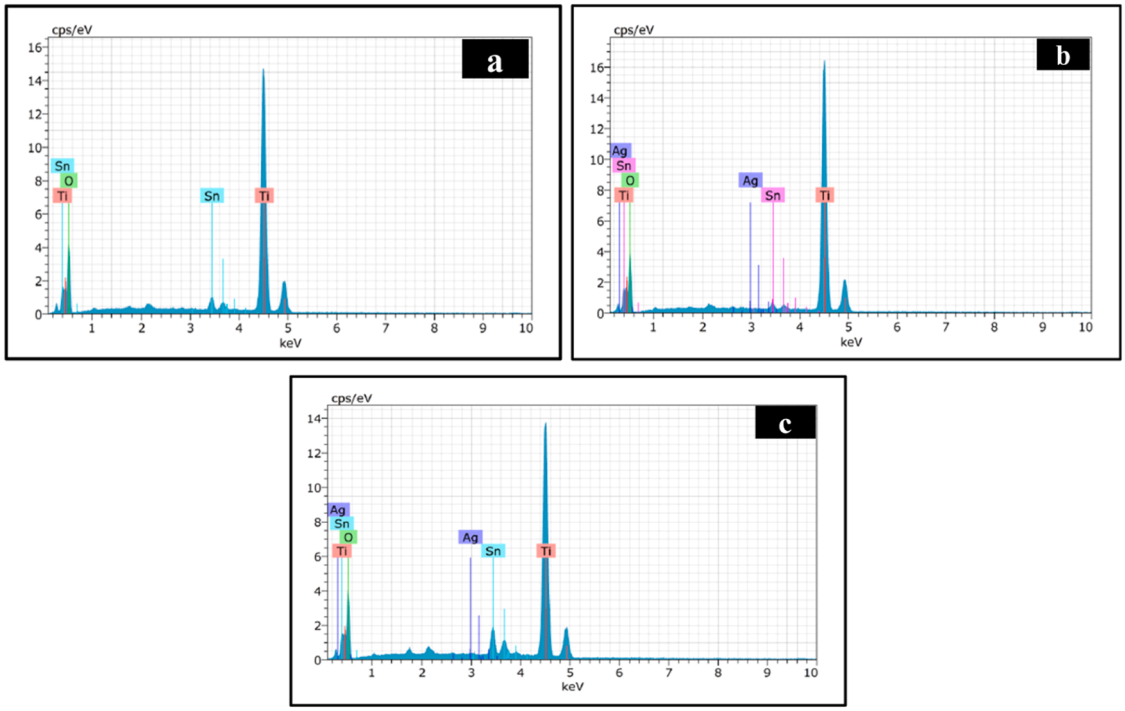

Fig. 2. Energy-Dispersive X-ray spectra of (a) Un-doped, (b) 3 mmol % Ag-doped TiO_2 nanomaterials and (c) 7 mmol % Ag-doped TiO_2 nanomaterials.

Table 2
Atomic percentage of elements present in Un-doped, 3 mmol % Ag-doped and 7 mmol % Ag-doped TiO_2 nanomaterials.

Element	Un-doped TiO_2 (at. %)	3 mmol % Ag-doped TiO_2 (at. %)	7 mmol % Ag-doped TiO_2 (at. %)
Ti	26.01	28.67	25.77
O	73.26	70.89	72.58
Sn	0.73	0.43	1.63
Ag	–	0.01	0.02

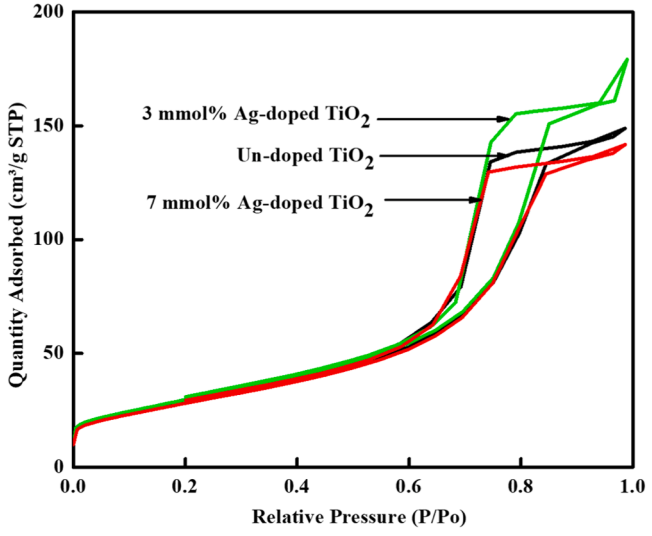

Fig. 3. N_2 adsorption-desorption isotherm of Un-doped TiO_2, 3 mmol % Ag-doped TiO_2 and 7 mmol % Ag-doped TiO_2 nanomaterials.

Table 3
Surface characteristic information of Un-doped, 3 mmol % Ag-doped and 7 mmol % Ag-doped TiO_2 nanomaterials.

Nanomaterial	BET surface area (m^2/g)	Pore volume (cm^3/g)	Adsorption average pore diameter (Å)	Desorption average pore diameter (Å)
Un-doped TiO_2	104.715	0.230	87.996	85.866
3 mmol % Ag-doped TiO_2	106.888	0.277	103.718	94.816
7 mmol % Ag-doped TiO_2	101.421	0.219	86.462	84.439

doping of Silver into TiO_2 nanomaterial. The appearance of Sn in EDX mapping could be justified as the said nanomaterials were coated on FTO glass substrates and employed for this analysis.

4.1.3. *Brunauer-Emmett-Teller (BET) analysis*

In order to investigate the effect of Ag doping on surface area of TiO_2 nanomaterials, Nitrogen adsorption-desorption analysis was carried out and the specific surface area of the nanomaterials was calculated by BET method. Fig. 3 represents a type IV N_2 adsorption-desorption isotherm of un-doped TiO_2, 3 mmol % Ag-doped TiO_2 and 7 mmol % Ag-doped TiO_2 according to the IUPAC physisorption isotherm classification and H2 hysteresis loop at the higher relative pressure indicates the large mesoporous character. Table 3 indicates the pore volume estimated at P/Po = 0.98 and pore diameters estimated using the BJH model for undoped and the selected Ag-doped TiO_2 nanomaterials [25]. It was observed that the BET surface area of 3 mmol % Ag-doped TiO_2 (106.89 m^2/g) is slightly greater than that of the undoped TiO_2 (104.72 m^2/g). Further, it was noted that the 7 mmol % Ag-doped TiO_2 shows a reduction in BET surface area which may due to agglomeration of particles at high dopant loading.

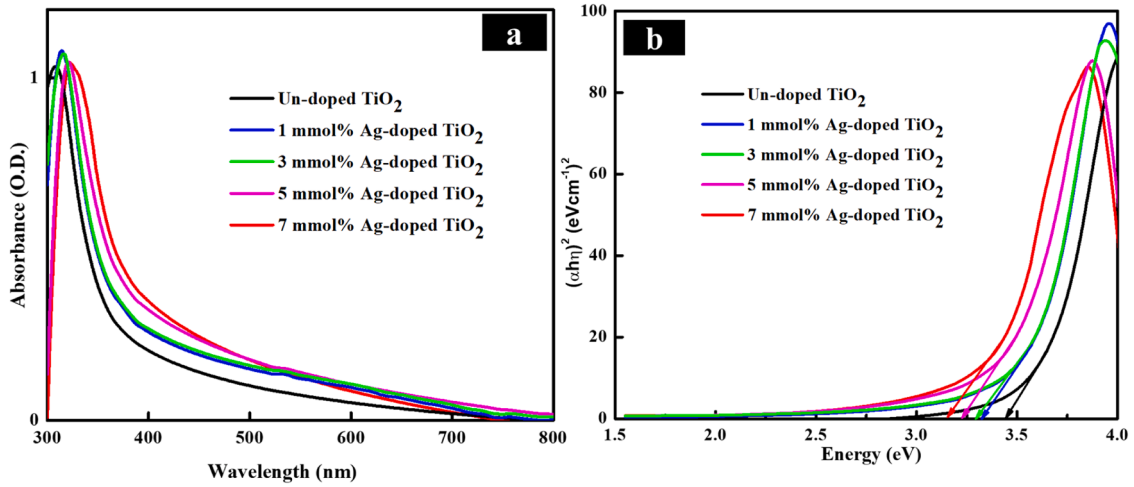

Fig. 4. (a) UV–Visible absorption spectra of Un-doped and Ag-doped TiO_2 nanomaterials coated films (b) Tauc plots for the corresponding nanomaterials.

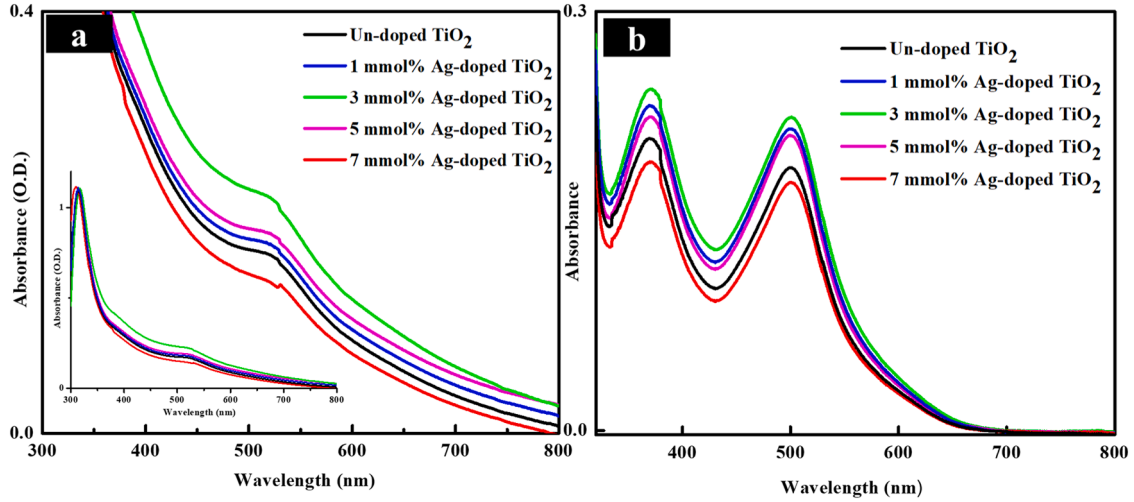

Fig. 5. UV–Visible absorption spectra of (a) dye adsorbed Un-doped & Ag-doped TiO_2 films (b) the desorbed dye in aqueous NaOH solution.

4.2. Optical characterization

4.2.1. UV–Visible spectroscopy

The optical properties of un-doped and Ag-doped TiO_2 nanomaterials were studied by UV–Visible spectroscopy. The corresponding UV- visible absorbance spectra of the said nanomaterials coated films are shown in Fig. 4(a) which exhibit absorption in the UV region of the electromagnetic radiation. The introduction of Silver into TiO_2 nanomaterials demonstrates a red shift in light absorption towards longer wavelength due to reduction in the bandgap value [26]. It allows the electrons to be excited with lower energy, thus absorbing more visible light.

The bandgaps of the synthesized nanomaterials coated films were estimated using the Tauc's formula, as provided below:

$$\alpha = A\frac{(h\nu - E_g)^n}{h\nu}$$

where α is the absorbance coefficient, $h\nu$ represents photon energy, A is a constant, E_g is the bandgap energy, and n is the exponential constant index. The value of n depends on the nature of the transition, with n being 1/2 for directly allowed transition and 2 for indirectly allowed transition. Accordingly, the estimated bandgaps of un-doped and 1, 3, 5, 7 mmol % Ag-doped TiO_2 nanomaterials were determined as 3.42, 3.38, 3.28, 3.23, and 3.15 eV respectively as illustrated in Fig. 4(b). The reduction in the estimated bandgap values as a result of Ag doping may be due to the formation of 4*d* state of Ag between the valance band and conduction band of TiO_2 and the subsequent movement of electrons between the Ag 4*d* state and the conduction band of TiO_2 [27,17].

The effect of incorporating Silver into TiO_2 nanomaterial on the adsorption of N719 dye was also investigated. This involved immersing both Ag-doped TiO_2 and un-doped TiO_2 films separately in the N719 dye overnight, followed by measuring the absorbance of the resulting dye adsorbed films using UV–Visible spectroscopy. Fig. 5(a) reveals enhanced dye adsorption capacity of the Ag-doped TiO_2 up to 3 mmol % of Silver dopant likely due to the expanded surface area of Ag-doped TiO_2 films; then, the dye adsorption gradually decreases on further increase in the dopant concentration. This aligns well with the recorded J_{SC} values of the devices constructed using the aforementioned dye-coated films. Subsequently, the dye desorption study was carried out by immersing each of the same films previously saturated with dye into a 3 mL of 1 N aqueous NaOH solution overnight. Then, the dye released into the NaOH solution was analyzed using UV–Visible spectroscopy. Fig. 5(b) shows the absorbance of the dye molecules desorbed from the respective nanomaterials and confirms the previously observed phenomenon.

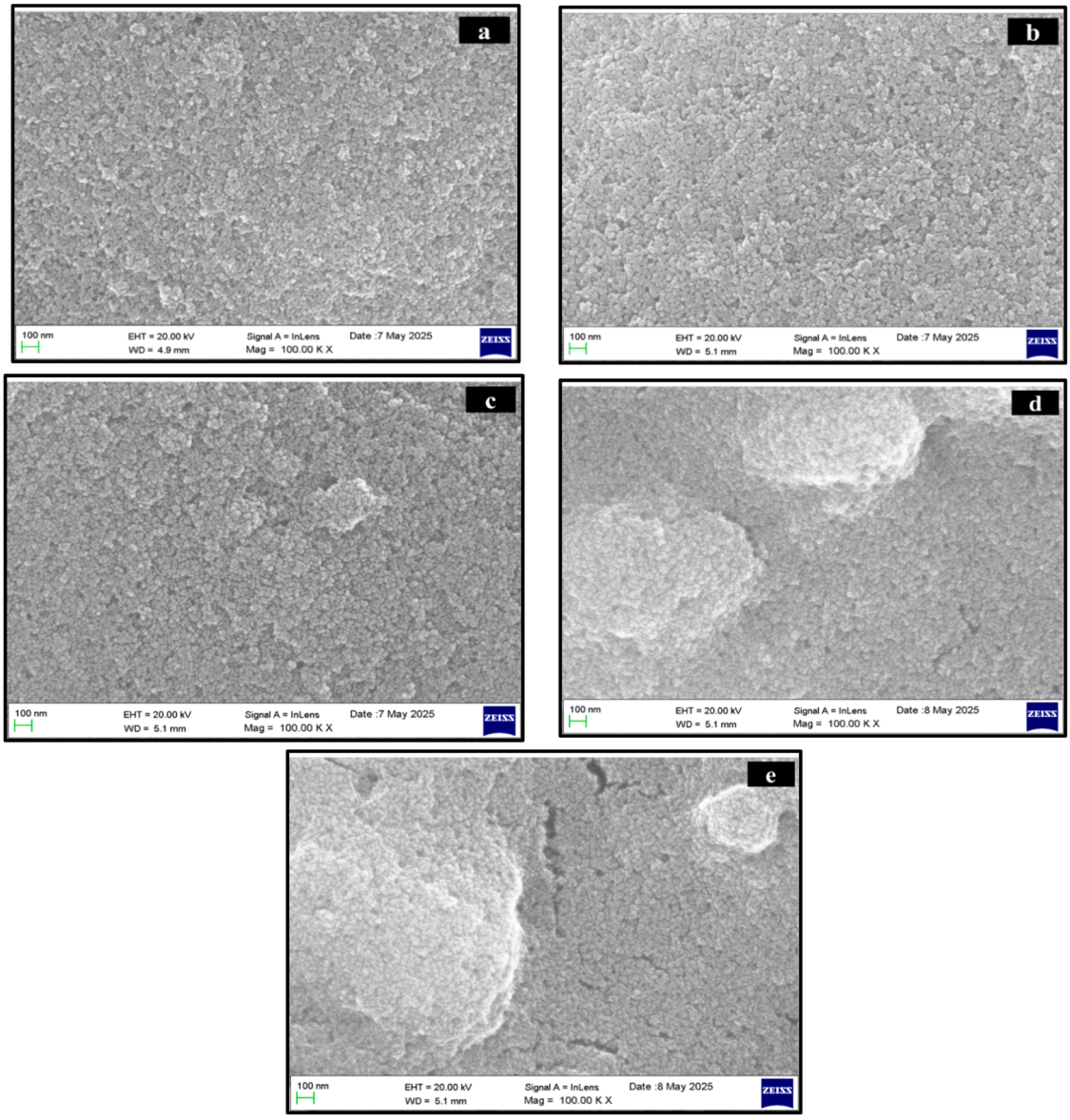

Fig. 6. Field Emission Scanning Electron Microscopic (FESEM) images of (a) Un-doped TiO_2, (b) 1 mmol % Ag-doped TiO_2, (c) 3 mmol % Ag-doped TiO_2, (d) 5 mmol % Ag-doped TiO_2, and (e) 7 mmol % Ag-doped TiO_2 films.

4.3. Morphological characterization

4.3.1. Field-Emission scanning electron microscopy (FESEM)

The surface morphologies of the synthesized films were examined using Field-Emission Scanning Electron Microscopy (FESEM). Fig. 6(a) illustrates the FESEM image of un-doped TiO_2 film which possesses a dense and relatively uniform layer composed of closely packed nanoparticles. With the introduction of silver at a low concentration of 1 mmol % (Fig. 6(b)), morphology similar to that of the un-doped sample is observed which is characterized by a homogeneous distribution of fine particles. A network of interconnected nanoparticles is revealed in the 3 mmol % Ag-doped TiO_2 film (Fig. 6(c)), which exhibited the best performance in the Dye-Sensitized Solar Cell studies, suggesting that improved inter-particle contact has been achieved. As the silver doping concentration increases to 5 mmol % (Fig. 6(d)) and 7 mmol % (Fig. 6 (e)), a progressive increase in particle agglomeration is observed, resulting in the formation of larger clusters and a less uniform surface texture. This agglomeration at higher doping levels is believed to reduce the effective surface area available for dye adsorption, potentially accounting for the reduced performance in the corresponding DSSCs [11]. Through high-resolution FESEM analysis, the evolution of film morphology with increasing silver content is clearly visualized with the optimal structure identified at the 3 mmol % Ag doping level.

4.4. Photovoltaic performance

4.4.1. J-V measurement

The photovoltaic characteristics of the un-doped and 1, 3, 5 and 7 mmol % Ag-doped TiO_2 N719 dye, were evaluated using imidazolium iodide/ triiodide electrolyte and Pt counter electrode. The J-V measurement was carried out using Keithley-2400 source meter (Peccell-PEC-L12, Japan) under simulated irradiation at an intensity of 100 $mWcm^{-2}$, employing an AM 1.5 filter (1 sun). The power conversion efficiency (η) of a DSSC is correlated with short-circuit current density (J_{SC}), open-circuit voltage (V_{OC}), fill factor (*FF*), and the incident light intensity (P_{in}) as shown below:

$$\eta = \frac{J_{sc}\ x\ V_{oc}\ x\ FF}{P_{in}} X\ 100\ \%$$

The photovoltaic characteristics of DSSCs, assembled with un-doped

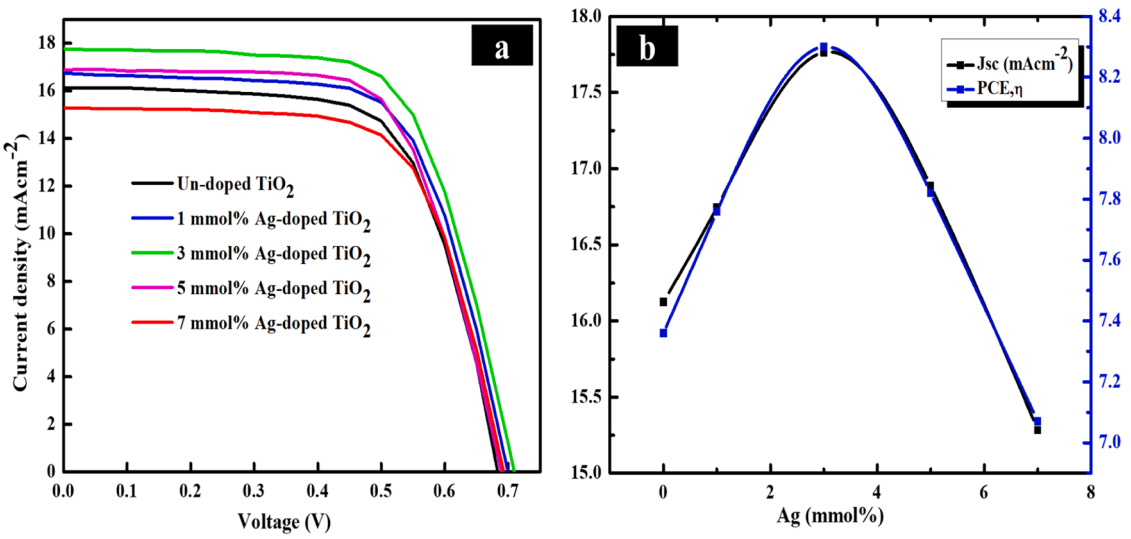

Fig. 7. (a) Current-Voltage (J–V) characteristics of the DSSCs assembled with Un-doped and Ag-doped TiO_2 photoelectrodes; (b) Variations in short-circuit current density (J_{SC}) and power conversion efficiency (η) with varied amounts of Ag dopant under illumination of intensity 100 $mWcm^{-2}$ with AM 1.5 filter.

Table 4
Current-Voltage (J–V) characteristics of the DSSCs assembled with Un-doped and Ag-doped TiO_2 photoelectrodes under illumination of intensity 100 $mWcm^{-2}$ with AM 1.5 filte.

Photoelectrode	J_{SC} ($mAcm^{-2}$)	V_{OC} (V)	FF	PCE, η (%)
Un-doped TiO_2	16.13	0.68	0.67	7.35
1 mmol % Ag-doped TiO_2	16.75	0.70	0.66	7.74
3 mmol % Ag-doped TiO_2	**17.76**	**0.71**	**0.66**	**8.32**
5 mmol % Ag-doped TiO_2	16.87	0.69	0.67	7.80
7 mmol % Ag-doped TiO_2	15.28	0.69	0.67	7.06

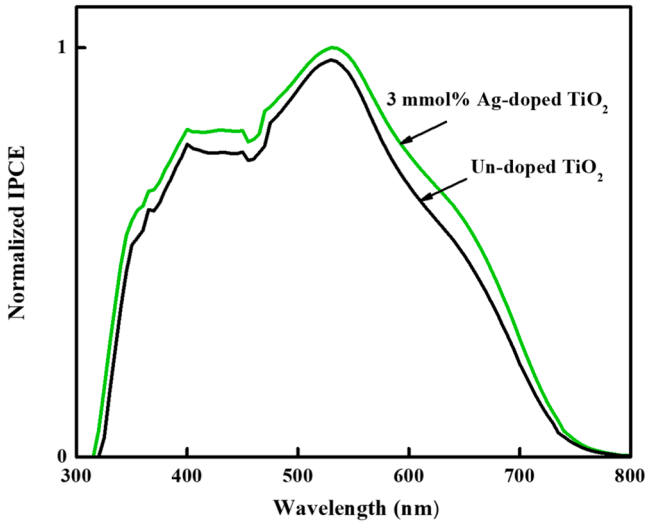

Fig. 8. Normalized IPCE Spectra of Un-doped and 3 mmol % Ag-doped TiO_2 based DSSCs.

and Ag-doped TiO_2 photoelectrodes, are illustrated in Fig. 7 and the related photovoltaic parameters are summarized in Table 4.

The J-V analyses demonstrate a notable improvement in the power conversion efficiency of DSSCs with 3 mmol % Ag-doped TiO_2 based photoelectrode. The said device showed PCE of 8.32 %, which was about 13 % greater than the device with un-doped TiO_2 (η = 7.35 %). This enhancement is primarily attributed to the increase in short-circuit current density (J_{SC}), with both fill factor (FF) and open-circuit voltage (V_{OC}) playing a relatively minor role in influencing the overall PCE. This significant upsurge in short-circuit current density resulted from improved light absorption and enhanced dye adsorption by the Ag-doped TiO_2 was confirmed by UV–Visible spectroscopy.

4.4.2. *Incident photon-to-current conversion efficiency (IPCE)*

The monochromatic incident photon-to-collected electron conversion efficiency (IPCE) represents the external quantum yield of a device and can be expressed as follows:

$$IPCE = (LHE)(\phi_{inj})(\eta_{el})$$

where **LHE** is the light harvesting efficiency, ϕ_{inj} is the charge injection yield and η_{el} is the charge collection efficiency.

Fig. 8 compares the IPCEs of DSSCs utilizing un-doped TiO_2 and 3 mmol % Ag-doped TiO_2. The DSSC employing 3 mmol % Ag-doped TiO_2 exhibits a superior IPCE compared to the DSSC utilizing un-doped TiO_2. The rise in the IPCE value well aligns with the findings from the UV–Visible absorbance spectra of dye-adsorbed TiO_2 films and desorbed dye and increased current–voltage performance of 3 mmol % Ag-doped TiO_2 based DSSC.

4.4.3. *Electrochemical impedance spectroscopy (EIS)*

The EIS measurements were carried out using two electrode system within a frequency range of 1×10^6 to 1×10^{-2} Hz in the dark mode with the applied voltage of 0.5 V using electrochemical workstation (Bio-Logic, SP-150e, France). The photoelectrodes fabricated from un-doped TiO_2 as well as TiO_2 doped with optimum & maximum quantities of Silver were employed to investigate the impact of interfacial resistance on the power conversion efficiency of the corresponding Dye-Sensitized Solar Cells.

Fig. 9(a) depicts the Nyquist plots of the DSSCs assembled with un-doped TiO_2, 3 mmol % Ag-doped TiO_2, and 7 mmol % Ag-doped TiO_2 based photoelectrodes in dark. In general, the electrochemical impedance spectrum of a liquid electrolyte based DSSC exhibits three semicircles associated with the interfacial resistance and the oxidation–reduction reactions occurring in the DSSC under dark condition. The semicircle in the highest frequency region correlates with the charge transfer resistance (R_{ct}) of the Pt/electrolyte and FTO/TiO_2 interfaces, the next semicircle in the intermediate frequency region is related to the charge recombination resistance (R_{rec}) at the TiO_2/dye/electrolyte interface and the third semicircle in the lowest frequency

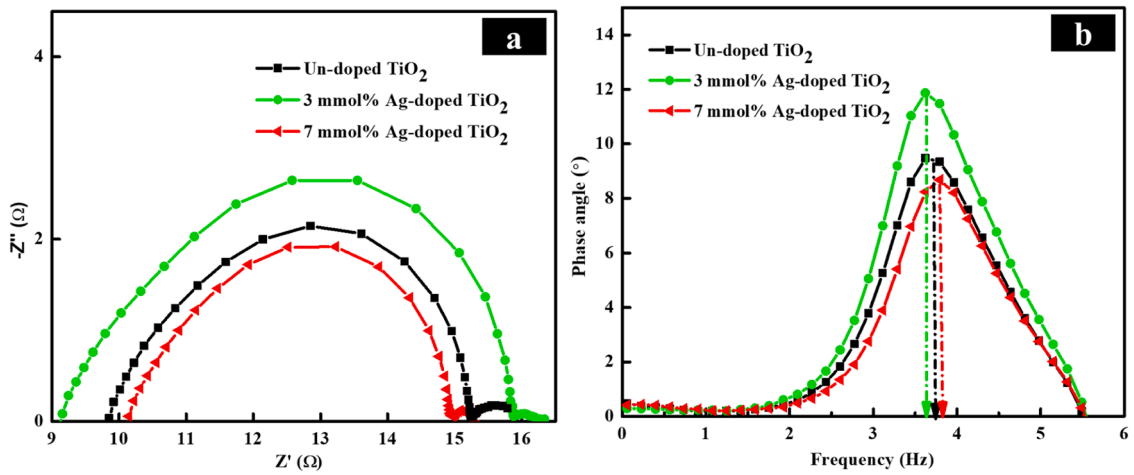

Fig. 9. (a) Nyquist plots of the DSSCs assembled with Un-doped TiO_2, 3 mmol % Ag-doped TiO_2, and 7 mmol % Ag-doped TiO_2 based photoelectrodes in dark and (b) Bode plots of the same devices.

Table 5
EIS parameters, J_{SC} and, V_{OC} of the SSCs assembled with Un-doped TiO_2, 3 mmol % Ag-doped TiO_2, and 7 mmol % Ag-doped TiO_2 photoelectrodes in dark.

Photoelectrode	R_s	R_{ct}	R_{rec}	f_{max} (Hz)	T_e (ms)	J_{SC} (mAcm^{-2})	V_{OC} (V)
Un-doped TiO_2	9.95	1.17	4.09	3.76	42.37	16.13	0.68
3 mmol % Ag-doped TiO_2	9.27	1.35	5.21	3.61	44.07	17.76	0.71
7 mmol % Ag-doped TiO_2	10.23	0.94	3.73	3.83	41.56	15.28	0.69

region is associated with Nernst diffusion process in the electrolyte. The series resistance (R_S) could be obtained from the lower extreme intersection point of the semicircle in the highest frequency region at the horizontal axis of Nyquist plot [28].

As illustrated in Table 5, the device with 3 mmol % Ag-doped TiO_2 exhibits the highest charge recombination resistance among the tested devices, indicating superior PV performance. These findings align closely with the increased J_{SC} values and power conversion efficiency (η) values of the fabricated devices.

Fig. 9(b) depicts the Bode plots of the devices with un-doped TiO_2, 3 mmol % Ag-doped TiO_2, and 7 mmol % Ag-doped TiO_2 based photoelectrodes and the electron life time (Te), which is also known as the charge recombination time in the dark, was calculated using the following equation:

$$T_e = \frac{1}{2\pi f_{max}}$$

where f_{max} is the maximum frequency corresponding to the peak. In the present study, the photoelectrode with 3 mmol % Ag-doped TiO_2 demonstrated the longest charge recombination time, indicating that incorporation of Ag into TiO_2 effectively suppresses the charge recombination rate in DSSCs.

The increased J_{SC} value observed for 3 mmol % Ag-doped TiO_2 sample (Table 5) suggests an increased recombination resistance compared to the un-doped TiO_2. This could be attributed to the presence of silver dopant within the photoelectrode, which serves to shorten the electron transport pathways. Consequently, efficient electron transfer from the TiO_2 layer to the FTO glass substrate is facilitated, and overall efficiency of the device is enhanced [29]. The increased V_{OC} value observed for 3 mmol % Ag-doped TiO_2 suggests that charge recombination was reduced due to an equilibrium established between the Fermi levels of TiO_2 and Ag. This equilibrium forms a Schottky barrier, causing

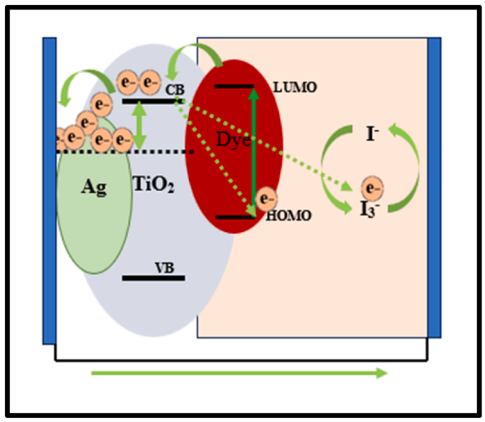

Fig. 10. Effect of Ag-doping on charge transfer within TiO_2 based DSSC framework.

a significant accumulation of electrons on the surface of the Ag and shifting the Fermi level closer to the conduction band of TiO_2. This Schottky barrier promotes electron flow from the Ag to the conduction band of TiO_2 through a fast interfacial charge transfer process, enhancing photocurrent generation and preventing the reverse flow of electrons from TiO_2 to the dye or electrolyte, leading to an increase in electron density in the TiO_2 conduction band [30,31]. Fig. 10 illustrates the effect of Ag-doping on charge transfer within the TiO_2-based DSSC framework. When concentration of Ag increases, the active sites become covered by a substantial amount of silver, resulting in reduced carrier generation. Additionally, a high loading of Ag on the TiO_2 surface creates Ag recombination centres for photoelectrons and holes, resulting in the reduction of electron lifetime and decrease in J_{SC} and V_{OC} values; hence, the overall power conversion efficiency of the DSSC is severely affected [19,32,33].

Table 6 compares the PCEs of Ag-doped TiO_2 photoelectrode-based devices reported in the literature with the present study. Although the amount of Ag dopant, method of photoelectrode preparation, and other factors vary, the Ag-doped TiO_2 nanomaterial employed in the current study is shown to be more efficient for DSSC application.

5. Conclusion

In this study, un-doped and Ag-doped TiO_2 nanomaterials were synthesized using a hydrothermal method, and the corresponding DSSCs

Table 6
Comparison of the power conversion efficiencies of Ag-doped TiO_2 photoelectrode based DSSCs.

Amount of Ag Dopant	Source of TiO_2	Procedure for Nanomaterial Synthesis	Method of Photoelectrode Preparation	PCE (η, %)	Reference
1 %	TTIP	modified Sol–Gel route	Doctor blading	0.40	[19]
1 %	TTIP	Chemical synthesis	Dip coating	4.40	[18]
10 %	TTIP	Sol-Gel method	Doctor blading	5.60	[21]
1×10^{16} atoms/cm^2	P25 TiO_2	–	Screen printing	5.85	[17]
0.1 M	TTIP	Hydrothermal method	Doctor blading	6.44	[34]
2 %	P25 TiO_2	–	Radiolytic reduction of Ag+ ion	7.73	[20]
3 mmol %	TTIP	Hydrothermal Treatment followed by steam hydrolysis of TTIP	Spray pyrolysis	8.30	Current study

were fabricated via spray pyrolysis. XRD analysis confirmed the anatase phase for both un-doped and Ag-doped TiO_2 with a reduction in crystallite size upon Ag doping, which is expected to enhance electron transport and reduce recombination. EDX spectra confirmed the successful doping of silver. UV–Visible spectra demonstrated a red shift for Ag-doped TiO_2 indicating enhanced light absorption in the visible region that is crucial for improved solar energy harvesting. SEM images showed spherical particles, with agglomeration at higher Ag dopant concentrations. J-V measurements revealed that DSSC with 3 mmol % Ag-doped TiO_2 photoelectrode had achieved a 13 % higher power conversion efficiency (PCE = 8.32 %) compared to the control (PCE = 7.35 %), primarily due to an increased short-circuit current density (J_{SC}). This enhancement was attributed to reduced charge recombination and improved visible light absorption, as corroborated by EIS and UV–Visible spectral analyses. Overall, the findings suggest that Ag doping on TiO_2 photoelectrode can significantly improve the performance of DSSCs, offering a promising approach for developing cost-effective and efficient solar energy devices. To further enhance and understand the short-circuit current density (J_{SC}), future research should focus on both material-level and device-level strategies. At the material level, the incorporation of plasmonic nanoparticles or light-scattering layers could also enhance light absorption and carrier generation. At the device level, engineering the interface between active layers and electrodes to minimize energy barriers and improve charge extraction is essential. Additionally, employing advanced characterization techniques such as transient photovoltage/current measurements and time-resolved spectroscopy can offer deeper insight into charge generation, transport, and recombination mechanisms. These combined efforts will contribute not only to improved J_{SC} values but also to a comprehensive understanding of the underlying photo-physical processes.

CRediT authorship contribution statement

Piranave Sritharan: Writing – original draft, Visualization, Software, Methodology, Investigation, Formal analysis, Data curation. **Meena Senthilnanthanan:** Writing – review & editing, Validation, Supervision, Project administration, Funding acquisition, Data curation, Conceptualization. **Punniamoorthy Ravirajan:** Writing – review & editing, Validation, Supervision, Funding acquisition, Data curation, Conceptualization. **Dhayalan Velauthapillai:** Writing – review & editing, Validation, Supervision, Data curation, Conceptualization. **Gamaralalage Rajanya Asoka Kumara:** Writing – review & editing, Resources, Methodology. **Balraju Palanisamy:** Writing – review & editing, Methodology.

Declaration of competing interest

The authors declare that they have no known competing financial interests or personal relationships that could have appeared to influence the work reported in this paper.

Acknowledgement

The authors acknowledge the financial assistance provided by the National Research Council of Sri Lanka (NRC Grant No.: 20-111) and NORPART2021/10095, Higher Education and Research Collaboration on Nanomaterials for Clean Energy Technologies 2.0 (HRNCET 2.0)

Supplementary materials

Supplementary material associated with this article can be found, in the online version, at doi:10.1016/j.chphi.2025.100910.

Data availability

Data will be made available on request.

References

[1] V. Madurai Ramakrishnan, et al., Performance of TiO2 nanoparticles synthesized by microwave and solvothermal methods as photoanode in dye-sensitized solar cells (DSSC), Int. J. Hydrogen Energy 45 (51) (2020) 27036–27046, https://doi.org/10.1016/j.ijhydene.2020.07.018.
[2] E. Kouhestanian, M. Ranjbar, S.A. Mozaffari, H. Salaramoli, Investigating the effects of thickness on the performance of ZnO-based DSSC, Prog. Color. Color. Coatings 14 (2) (2021) 101–112.
[3] N. Puspitasari, et al., Fabrication and characterization of TiO2 & SnO2 nanoparticles as a photoanodes in dye sensitized solar cell, J. Phys. Conf. Ser. 1153 (1) (2019), https://doi.org/10.1088/1742-6596/1153/1/012075.
[4] R. Panetta, A. Latini, I. Pettiti, C. Cavallo, Synthesis and characterization of Nb2O5 mesostructures with tunable morphology and their application in dye-sensitized solar cells, Mater. Chem. Phys. 202 (2017) 289–301, https://doi.org/10.1016/j.matchemphys.2017.09.030.
[5] M. Irfan, M.I. Khan, M. Al Huwayz, and N. Alwadai, "Synthesis, characterization, and photodegradation assessment of Ni and Cd-doped TiO 2 nanocrystals via sol-gel method for methylene blue under sunlight," vol. 19, no. 2, pp. 953–966, 2024.
[6] B. Roose, S. Pathak, U. Steiner, Doping of TiO2 for sensitized solar cells, Chem. Soc. Rev. 44 (22) (2015) 8326–8349, https://doi.org/10.1039/c5cs00352k.
[7] V. Gayathri, I.J. Peter, N. Rajamanickam, K. Ramachandran, Improved performance of dye-sensitized solar cells by Cr doped TiO2 nanoparticles, Mater. Today Proc 35 (February) (2019) 23–26, https://doi.org/10.1016/j.matpr.2019.05.381.
[8] B. Yacoubi, L. Samet, J. Bennaceur, A. Lamouchi, R. Chtourou, Properties of transition metal doped-titania electrodes: impact on efficiency of amorphous and nanocrystalline dye-sensitized solar cells, Mater. Sci. Semicond. Process. 30 (2015) 361–367, https://doi.org/10.1016/j.mssp.2014.10.035.
[9] N. Kanjana, W. Maiaugree, P. Poolcharuansin, P. Laokul, Synthesis and characterization of Fe-doped TiO2 hollow spheres for dye-sensitized solar cell applications, Mater. Sci. Eng. B Solid-State Mater. Adv. Technol. 271 (May) (2021) 115311, https://doi.org/10.1016/j.mseb.2021.115311.
[10] R. Krishnapriya, C. Nizamudeen, B. Saini, M.S. Mozumder, R.K. Sharma, A.H. I. Mourad, MOF-derived Co2+-doped TiO2 nanoparticles as photoanodes for dye-sensitized solar cells, Sci. Rep. 11 (1) (2021) 1–12, https://doi.org/10.1038/s41598-021-95844-4.
[11] T. Rajaramanan, D. Velauthapillai, P. Ravirajan, M. Senthilnanthanan, A facile impregnation synthesis of Ni-doped TiO2 nanomaterials for dye-sensitized solar cells, J. Mater. Sci. Mater. Electron. 34 (10) (2023) 1–12, https://doi.org/10.1007/s10854-023-10347-4.
[12] K. Sahu, M. Dhonde, V.V.S. Murty, Microwave-assisted hydrothermal synthesis of Cu-doped TiO2 nanoparticles for efficient dye-sensitized solar cell with improved open-circuit voltage, Int. J. Energy Res. 45 (4) (2021) 5423–5432, https://doi.org/10.1002/er.6169.
[13] T. Rajaramanan, et al., Cost effective solvothermal method to synthesize zn-doped tio2 nanomaterials for photovoltaic and photocatalytic degradation applications, Catalysts 11 (6) (2021), https://doi.org/10.3390/catal11060690.
[14] T. Rajaramanan, M. Natarajan, P. Ravirajan, M. Senthilnanthanan, D. Velauthapillai, Ruthenium (Ru) doped titanium dioxide (P25) electrode for dye sensitized solar cells, Energies 13 (7) (2020) 1–12, https://doi.org/10.3390/en13071532.
[15] M.C. Kao, J.H. Weng, C.H. Chiang, K.H. Chen, D.Y. Lin, T.K. Kang, Effect of tungsten doping on the properties of titanium dioxide dye-sensitized solar cells, Energies 17 (20) (2024), https://doi.org/10.3390/en17205118.

[16] A.M. Sharif, et al., Green synthesis of pristine and Ag-doped TiO2 and investigation of their performance as photoanodes in dye-sensitized solar cells, Materials (Basel) 16 (17) (2023), https://doi.org/10.3390/ma16175731.
[17] J. Luo, et al., Effects of Ag-ion implantation on the performance of DSSCs with a tri-layer TiO2 film, RSC Adv 4 (99) (2014) 56318–56322, https://doi.org/10.1039/c4ra09221j.
[18] K. Usha, P. Kumbhakar, B. Mondal, Effect of Ag-doped TiO2 thin film passive layers on the performance of photo-anodes for dye-sensitized solar cells, Mater. Sci. Semicond. Process. 43 (2016) 17–24, https://doi.org/10.1016/j.mssp.2015.11.015.
[19] A.K. Gupta, P. Srivastava, L. Bahadur, Improved performance of Ag-doped TiO2 synthesized by modified sol–gel method as photoanode of dye-sensitized solar cell, Appl. Phys. A Mater. Sci. Process. 122 (8) (2016), https://doi.org/10.1007/s00339-016-0241-2.
[20] S. Sardar, et al., Enhanced photovoltage in DSSCs: synergistic combination of a silver modified TiO2 photoanode and a low cost counter electrode, RSC Adv. 6 (40) (2016) 33433–33442, https://doi.org/10.1039/c6ra01863g.
[21] K. Balachandran, T. Kalaivani, D. Thangaraju, S. Mageswari, M.S.V. Senan, A. Preethi, Fabrication of photoanodes using sol-gel synthesized Ag-doped TiO2 for enhanced DSSC efficiency, Mater. Today Proc 37 (Part 2) (2020) 515–521, https://doi.org/10.1016/j.matpr.2020.05.485.
[22] K.D. Mudiyanselage, Sakunthala Pubudu Kumari Kumarasinghe, B. C. Karunarathne, S.P. Dunuweera, R.M. Gamini Rajapakse, K. Tennakone, G. R. Asoka Kumara, Impact of 4-tertiary-butylpyridine in imidazolium iodide/triiodide redox couple-based dye-sensitized solar cells, ACS Appl. Energy Mater. (2021), https://doi.org/10.1021/acsaem.1c01587.
[23] M. Irfan, A.A. Haidry, Multifunctional Cu–TiO2 porous nano-structures via post-synthesis LASER treatment for boosting energy storage and photocatalytic applications, J. Indian Chem. Soc. 102 (5) (2025) 101683, https://doi.org/10.1016/j.jics.2025.101683.
[24] M. Irfan, et al., Improving photocatalytic efficiency of ZnO nanoflowers through gold incorporation for rhodamine B photodegradation, Opt. Mater. (Amst). 154 (May) (2024) 115681, https://doi.org/10.1016/j.optmat.2024.115681.
[25] A. Sirivallop, T. Areerob, S. Chiarakorn, Enhanced visible light photocatalytic activity of N and Ag doped and co-doped TiO2 synthesized by using an in-situ solvothermal method for gas phase ammonia removal, Catalysts 10 (2) (2020), https://doi.org/10.3390/catal10020251.
[26] K.B. Bhojanaa, M. Ramesh, A. Pandikumar, Complementary properties of silver nanoparticles on the photovoltaic performance of titania nanospheres based photoanode in dye-sensitized solar cells, Mater. Res. Bull. 122 (2020) 110672, https://doi.org/10.1016/j.materresbull.2019.110672.
[27] M. Guo, J. Du, First-principles study of electronic structures and optical properties of Cu, Ag, and Au-doped anatase TiO 2, Phys. B Condens. Matter 407 (6) (2012) 1003–1007, https://doi.org/10.1016/j.physb.2011.12.128.
[28] J. Zhao, et al., Efficient light-scattering functionalized TiO 2 photoanodes modified with cyanobiphenyl-based benzimidazole for dye-sensitized solar cells with additive-free electrolytes, J. Mater. Chem. 22 (35) (2012) 18380–18386, https://doi.org/10.1039/c2jm32607h.
[29] A. Ranjitha, N. Muthukumarasamy, M. Thambidurai, D. Velauthapillai, Enhanced photovoltaic performance of quantum dot sensitized solar cells with Ag-doped TiO2 nanocrystalline thin films, J. Mater. Sci. Mater. Electron. 25 (6) (2014) 2724–2729, https://doi.org/10.1007/s10854-014-1935-x.
[30] Y. Xu, H. Zhang, X. Li, W. Wang, J. Li, Ag-encapsulated Single-Crystalline Anatase TiO2 nanoparticle photoanodes for enhanced dye-sensitized solar cell performance, J. Alloys Compd. (2016), https://doi.org/10.1016/j.jallcom.2016.10.236.
[31] P. Christopher, D.B. Ingram, S. Linic, Enhancing photochemical activity of semiconductor nanoparticles with optically active Ag nanostructures: photochemistry mediated by Ag surface plasmons, J. Phys. Chem. C 114 (19) (2010) 9173–9177, https://doi.org/10.1021/jp101633u.
[32] N. Asim, et al., A review on the role of materials science in solar cells, Renew. Sustain. Energy Rev. 16 (8) (2012) 5834–5847, https://doi.org/10.1016/j.rser.2012.06.004.
[33] J. Li, et al., Silver nanoparticle doped TiO2 nanofiber dye sensitized solar cells, Chem. Phys. Lett. 514 (1–3) (2011) 141–145, https://doi.org/10.1016/j.cplett.2011.08.048.
[34] Y.X. Dong, X.L. Wang, E.M. Jin, S.M. Jeong, B. Jin, S.H. Lee, One-step hydrothermal synthesis of Ag decorated TiO2 nanoparticles for dye-sensitized solar cell application, Renew. Energy 135 (2019) 1207–1212, https://doi.org/10.1016/j.renene.2018.12.062.